JAAS

Accepted Manuscript

This is an *Accepted Manuscript*, which has been through the Royal Society of Chemistry peer review process and has been accepted for publication.

Accepted Manuscripts are published online shortly after acceptance, before technical editing, formatting and proof reading. Using this free service, authors can make their results available to the community, in citable form, before we publish the edited article. We will replace this *Accepted Manuscript* with the edited and formatted *Advance Article* as soon as it is available.

You can find more information about *Accepted Manuscripts* in the Information for Authors.

Please note that technical editing may introduce minor changes to the text and/or graphics, which may alter content. The journal's standard Terms & Conditions and the Ethical guidelines still apply. In no event shall the Royal Society of Chemistry be held responsible for any errors or omissions in this *Accepted Manuscript* or any consequences arising from the use of any information it contains.

ROYAL SOCIETY OF CHEMISTRY

www.rsc.org/jaas

Molybdenum Isotopic Analysis with Negative Thermal Ionization Mass Spectrometry (N-TIMS): Effects on Oxygen Isotopic Composition

Yuichiro NAGAI*[1] and Tetsuya YOKOYAMA[1]

1: Department of Earth and Planetary Sciences, Tokyo Institute of Technology, Ookayama, Tokyo 152-8551, Japan

* Corresponding author: (yuichiro.nagai@geo.titech.ac.jp)

September 8th, 2015

Revised version: January 30th, 2016

Submitted to *Journal of Analytical Atomic Spectrometry*

6924 words

Abstract

We developed a new, highly precise, and accurate Mo isotope analysis with thermal ionization mass spectrometry in negative ionization mode (N-TIMS). We discovered that the optimal condition to ionize Mo most efficiently into MoO_3^- was to load the Mo sample on a Re filament and cover the sample with $La(NO_3)_3$, thus yielding La/Mo = 5. To achieve highly precise Mo isotope analysis, determining the oxygen isotopic composition of MoO_3^- ion in each measurement by monitoring masses 149 ($^{100}Mo^{16}O_2{}^{17}O^-$) and 150 ($^{100}Mo^{16}O_2{}^{18}O^-$) ions and using the data for correcting for the O isotope interferences is important. After correcting the O isotopic interferences and performing mass-dependent fractionation during the TIMS measurement, the acquired Mo isotopic ratios yielded the following reproducibilities (2 SD): 47, 16, 10, 13, and 33 ppm for $^{92}Mo/^{96}Mo$, $^{94}Mo/^{96}Mo$, $^{95}Mo/^{96}Mo$, $^{97}Mo/^{96}Mo$, and $^{100}Mo/^{96}Mo$, respectively. The reproducibilities have been improved by 1.3–2.7 times compared to those obtained in previous studies using multi-collector inductively coupled plasma mass spectrometry. The accuracy of our technique was confirmed by measuring two synthesized solutions with enriched ^{92}Mo, ^{97}Mo, and ^{100}Mo abundances and two iron meteorites, i.e., Henbury (IIIAB) and Albion (IVA). Moreover, we determined positive Mo isotope anomalies for a new iron meteorite, Tambo Quemad (IIIAB). Our N-TIMS technique can be applied to the studies of nucleosynthetic isotope anomalies in extraterrestrial materials as well as mass-dependent Mo isotopic shift in environmental samples.

1. Introduction

Considerable improvements in mass spectrometry techniques over the last 15 years have enabled high precision measurements of nontraditional stable isotopes, including a unique transition element such as molybdenum (Mo). It has seven stable isotopes, ^{92}Mo, ^{94}Mo, ^{95}Mo, ^{96}Mo, ^{97}Mo, ^{98}Mo, and ^{100}Mo with averaged abundances of 14.8%, 9.23%, 15.9%, 16.7%, 9.56%, 24.2%, and 9.67%[1], respectively[1]. The Mo isotope system is useful in geochemistry, biogeosciences, and environmental sciences because of the potential isotopic fractionation during redox reactions. For example, mass-dependent Mo isotope fractionation at a level of a few permil was detected with multi-collector inductively coupled plasma mass spectrometry (MC-ICP-MS) in various types of marine sediments, including Mn-oxide-enriched sediments in oxic conditions[2,3], anoxic sediments[4,5], and euxinic sediments[2,6-8]. The individual Mo isotopic behaviors of black shales and banded iron formations under each of the redox conditions are studied to reveal a complicated oxidation history for the surface environment in the Archean and Paleoproterozoic[9,10]. Moreover, the isotopic fractionation of Mo was caused by N_2-fixing organisms because Mo plays an important role as a metal cofactor in enzymes[11]. This type of isotopic fractionation was reproduced by an experiment for Mo assimilation during nitrate reduction and atmospheric N_2 fixation in fresh water cyanobacterium cultures[12].

In contrast, nucleosynthetic isotope anomalies in extraterrestrial materials (i.e.,

mass-independent isotopic shifts from the terrestrial value) have been another intriguing application for Mo isotopes. Molybdenum isotopes in the universe were synthesized via stellar nucleosynthesis of the *s*-process (trace ^{94}Mo, ^{95}Mo, ^{96}Mo, ^{97}Mo, and ^{98}Mo), the *r*-process (^{95}Mo, ^{97}Mo, ^{98}Mo, and ^{100}Mo), and the *p*-process (^{92}Mo and ^{94}Mo)[13]. Multiple studies utilizing MC-ICP-MS have discovered nucleosynthetic Mo isotope anomalies in various types of meteorites[14,15], which suggest the existence of isotope heterogeneity for Mo in the early Solar System. Compared to Mo isotope anomalies for carbonaceous chondrites and iron meteorites, those for other non-carbonaceous meteorites such as Cr[16] were undetected because of the small degree of their Mo isotope deviations from terrestrial materials. Therefore, highly precise Mo isotope analysis is required to discriminate these marginal anomalies even if large amounts of samples are used.

Although Mo isotopic analyses have generally been performed with MC-ICP-MS, thermal ionization mass spectrometry (TIMS) is an alternative choice for enabling high precision Mo isotopic compositions in terrestrial and extraterrestrial materials. One of the advantages of TIMS is that the kinetic energy distribution of the thermally ionized beam is much smaller (~0.5 eV) than that of the ion beam generated via plasma ionization (~5 eV), minimizing the fluctuation of the ion beam intensity compared to MC-ICP-MS. This enables high-precision isotope ratio measurements for some elements at levels ≤10 ppm using new generation TIMS instruments (e.g., Nd[17] and W[18]).

In the 1960s, Mo isotope measurements were performed by TIMS with a Mo^+ ion

beam, resulting in an analytical precision of ±0.6% for each Mo ratio (^{i}Mo/^{100}Mo).[19] Such a large analytical uncertainty was caused by poor Mo ionization efficiency owing to its higher first ionization potential (7.1 eV) compared to elements such as Sr[20] (5.7 eV) and Nd[17] (5.5 eV) whose isotopic compositions are analyzed with high precision by TIMS. To avoid this problem, TIMS has been devised and successfully applied to a variety of elements including not only Mo but also those with higher first ionization potentials (e.g., W[21] and Os[22]). The N-TIMS technique has been applied to Mo isotope analysis since the early 2000s, resulting in the analytical precision of >44 ppm for ^{95}Mo/^{98}Mo[23]; however, these measurements were performed with previous generation TIMS instruments, which have an inferior analytical precision compared to current techniques such as MC-ICP-MS.[15,24] To date, Mo isotope analysis has rarely been performed using the latest generation TIMS instrument, nor has it been compared to the results of MC-ICP-MS measurements. As demonstrated by W isotope analysis[18], higher precision can be achieved with TIMS when stronger beam intensities are generated by loading the target element on a filament much larger than that which is normally applied.

In this study, we developed a method to enable highly precise Mo isotope analysis utilizing the latest generation TIMS instrument in negative ion mode. To improve the accuracy and precision of isotope analysis, we specifically focused on the variability of O isotopic compositions of Mo trioxide ion (MoO_3^-) during the N-TIMS measurements. Moreover, we present Mo isotope compositions in an extraterrestrial sample (iron

meteorite) for comparison with recent works conducted with MC-ICP-MS.

2. Experimental

2.1. Reagents and activators

Deionized water (18.2 MΩ cm^{-1}) was prepared using a Milli-Q Integral 5 (Merck-Millipore Corp.) water purification system. Electronics industry (EL) grade 12 M HCl, 16 M HNO_3 (Mitsubishi Chem.) and 30 M HF of atomic absorption spectrometry (AAS) grade (Kanto Chem. Co. Ltd.) were distilled once using a two-bottle Teflon distillation system (referred to as 1D HCl, 1D HNO_3, and 1D HF, respectively).

Ca, La, and Cd standard solutions prepared in aqueous nitrate media for atomic absorption spectrometry (1000 μg/g; Kanto Chem. Co. Ltd.) were used to make activators, which helped enhance the ionization efficiency of MoO_3^- ions in the TIMS. In this study, we tested the following four activators: i) 1000 μg/g $Ca(NO_3)_2$ in 0.4 M HNO_3, ii) 1000, 5000, 10000, 15000, 20000, and 30000 μg/g $La(NO_3)_3$ in 1 M HNO_3, iii) 5000 μg/g $La(NO_3)_3$ + 5000 μg/g $Gd(NO_3)_3$ in 1 M HNO_3, and iv) 5000 μg/g $La(NO_3)_3$ + 5000 μg/g $Gd(NO_3)_3$ in 1 M HNO_3, coupled with 1000 μg/g $Ca(NO_3)_2$ in 0.4 M HNO_3.

2.2. Mo isotope standard and enriched isotopic solutions

A Mo standard solution for atomic absorption spectrometry (1000 μg/g in 1.3 M HNO_3-0.1 M HCl; Kanto Chemical Co., Inc.) was used as a running standard for Mo isotope analysis with N-TIMS. This solution, referred to as "Kanto-Mo," is considered to

have a representative terrestrial Mo isotopic composition, excluding the effect of mass-dependent fractionation.

To evaluate the accuracy of Mo isotope analysis using N-TIMS, two artificial samples with nonterrestrial Mo isotopic compositions (Mix-A and Mix-B) were prepared using three spike solutions that were enriched with ^{92}Mo, ^{97}Mo, and ^{100}Mo, respectively. The ^{92}Mo spike solution was prepared by dissolving 10.4 mg of ^{92}Mo-enriched (99.93%) metal powder, which was obtained from Isoflex USA Inc. The metal powder was first dissolved in 30 M HF and completely dried, and then re-dissolved in 16 M HNO_3 and heated to dryness. The residual was finally dissolved in 1 M HF–1 M HNO_3. The Mo concentration of the ^{92}Mo-enriched solution was determined by isotope dilution using a reference isotopic composition for ^{92}Mo-enriched metal, reported by Isoflex, and that for Kanto-Mo defined by IUPAC, resulting in a Mo concentration of 933 ng/g. Similarly, the ^{97}Mo and ^{100}Mo spike solutions were prepared from 9.14 and 8.04 mg of ^{97}Mo-enriched (94.19%) and ^{100}Mo-enriched (98.59%) metal powders, which were obtained from the Oak Ridge National Laboratory, and resulted in Mo concentrations of 656 and 582 ng/g, respectively. The isotopically enriched samples, Mix-A and Mix-B, were prepared by gravitationally mixing the Kanto-Mo and a mixture of three spike solutions (^{92}Mo:^{97}Mo:^{100}Mo = 1:0.4:0.5) in different proportions. The Mix-B sample contained approximately twice the amount of the spike mixture than that of the Mix-A sample. Note that the true isotopic compositions of Mix-A and Mix-B are difficult to determine by direct measurement with TIMS because the

effect of mass fractionation cannot be corrected without a known isotope ratio as a reference (e.g., $^{98}Mo/^{96}Mo$). Therefore, we estimated the isotopic compositions of Mix-A and Mix-B by the gravimetric calculations using the isotopic compositions of individual Mo spikes reported by Isoflex and Oak Ridge National Laboratory. Because the individual spike compositions reported are noncertified reference values, the accuracy of the estimated Mo isotope compositions in Mix-A and Mix-B are not as precise as ppm (10^{-6}) levels but are at percent (10^{-2}) levels.

2.3. Samples

The Mo isotopic composition of three terrestrial rocks, JB-3 (basalt, Mt. Fuji), JA-3 (andesite, Mt. Asama), and JR-2 (rhyolite, Wada Toge obsidian), as well as three iron meteorites, Tambo Quemado (IIIAB), Henbury (IIIAB), and Albion (IVA), were determined. The terrestrial rocks (~2 g) were dissolved in 90 mL Savillex Teflon beakers using HF-HNO_3 (2:1) at 120°C for a day, 150°C for 2 days, and 180°C for several days, followed by drying at 120°C. The Tambo Quemado sample was digested in a 1:2 mixture of concentrated HCl and HNO_3. From the sample solution, W was separated by a two-stage Hf-W chemical separation technique[25] and used in another project[26]. All the residual fractions excluding W were combined and dried at 120°C, which was dissolved in 0.5 M HF for 2 h in an ultrasonic bath. After centrifuging the sample solution, the supernatant was dried and dissolved in 1 mL 0.4 M HCl–0.5 M HF. The other iron meteorites excluding IIE

irons (~2g) were leached in 6 M HCl for 30 min at 120°C to obtain more purified fractions. The residual fractions were digested in 16 M HNO_3–12 M HCl at 120°C overnight. In contrast, IIE irons were dissolved in 16 M HNO_3–12 M HCl at 120°C overnight, with additional digestion in 16 M HNO_3–30 M HF to dissolve the silicates.

Mo was further purified by two-step anion exchange column chromatography using an Eichrom AG1X8 (200–400 mesh) with HF–HCl and HF–HNO_3 mixtures[27]. In the first step, the resin was charged in a polyethylene column, Muromac mini-column S-size (5 mmϕ, Muromachi Technos co.); cleaned sequentially with 6 M HCl, purified H_2O, 6 M HNO_3–3M HF, and purified H_2O; and finally conditioned using 0.4 M HCl–0.5M HF (2 mL). The sample solution (1 mL) was loaded on the column. The major elements (e.g., Fe), Ti–Zr–Hf and W, which could not be removed in the previous procedure, were successively removed by adding 0.4 M HCl–0.5 M HF (3 mL), 9 M HCl–0.05 M HF (5 mL), and 9 M HCl–1 M HF (10 mL), respectively. Subsequently, Mo was eluted with 6 M HNO_3–3 M HF (5 mL). The Mo fraction was dried and dissolved in 2 M HF (0.3 mL). In the second step, the Mo fraction was purified using a polypropylene column filled with 0.1 mL Eichrom 1X8. The resin was cleaned sequentially with 6 M HCl, purified H_2O, 6M HNO_3–3M HF, and purified H_2O. The resin bed was then conditioned using 0.4 M HCl–0.5 M HF. The Mo fraction was loaded on the cleaned resin bed, followed by the addition of 2 M HF (0.4 mL). Nb was subsequently eluted using 6 M HCl–0.1 M HF (2 mL), and Mo was finally obtained by adding 6 M HNO_3−3 M HF (1 mL).

The blank of this digestion and the chemical procedure was ~1 ng.

2.4. Mass Spectrometry

Molybdenum isotopic analysis was performed with N-TIMS using TRITON *plus* (Thermo Fisher Scientific Inc.) installed at the Tokyo Institute of Technology (Tokyo Tech). This instrument is equipped with nine Faraday cups with 10^{11} Ω amplifiers. A secondary electron multiplier (SEM) is placed behind the center Faraday cup.

2.4.1. Sample Loading

A zone-refined 99.999% Re filament (thickness = 0.0305 mm, width = 0.750 mm; H. Cross) was used in this study. Prior to sample loading, the Re filament was outgassed for 30 min at 4.5 A in a vacuum degassing system. The Mo sample (ca. 1000–4000 ng) was dissolved in 1 μL of 1.3 M HNO_3–0.1 M HCl and loaded on the filament. The sample solution was dried at 0.6 A and subsequently covered by 1 μL of the activator. As described above, we tested the following four activators, which were used in previous N-TIMS studies[18,23,28-29]: i) $Ca(NO_3)_2$, ii) $La(NO_3)_3$, iii) (La, Gd)$(NO_3)_3$, and iv) $Ca(NO_3)_2$ + (La, Gd)$(NO_3)_3$. The optimal choice of the activator will be discussed in Section 3.1.

2.4.2. Measurement of Mo isotope ratios

The sample filament was placed in an ion source under vacuum at $<1.5 \times 10^{-7}$ mbar

without oxygen bleeding. The sample filament was first heated at 250 mA/min until 1075°C, and then heated at 20 mA/min until 1150°C. After focusing the MoO_3^- ion beam, the filament continued to heat at 20 mA/min. The MoO_3^- ion beam intensity decreased slightly around 1160–1180°C, but started to increase above 1230–1280°C. The acquisition of Mo isotopes was started when the $^{94}MoO_3^-$ ion beam intensity exceeded 2.0 V (2.0×10^{-11} A).

In this study, we examined the static multicollection method. The cup configuration of the N-TIMS measurement is summarized in Table 1. Each measurement consists of 360 cycles (20 cycles/block × 18 blocks) of data acquisition with 16.777 s integration time. The amplifier gains were calibrated once at the start of each day. The baselines of amplifiers were measured for 30 s at the beginning of each block by deflecting the beam away from the detectors. The amplifier rotation system was applied to reduce the error due to amplifier gain calibration, in which an array of nine 10^{11} Ω amplifiers connected behind the nine Faraday cups was electrically rotated in each block using a relay matrix. The typical total analytical time including the sample heating was 3–4 h.

2.5. Data processing

In the N-TIMS measurement, Mo isotopic compositions were obtained by collecting Mo trioxide ions (MoO_3^-) using nine Faraday cups (Table 1). The intensities of the MoO_3^- ions collected by individual detectors do not reflect the true Mo isotopic composition

primarily because of the following two reasons: mass fractionation during the analysis (e.g., evaporation from filament) and oxygen isotopic interferences for $^{i}Mo^{16}O_3^-$ occurring as isobaric molecular ions such as $^{i-1}Mo^{16}O_2{}^{17}O^-$ and $^{i-2}Mo^{16}O_2{}^{18}O^-$. The latter issue is problematic because these isobars have very low abundances (0.2% and 0.04% for $^{i-1}Mo^{16}O_2{}^{17}O^-$ and $^{i-2}Mo^{16}O_2{}^{18}O^-$ relative to $^{i}Mo^{16}O_3^-$) and are difficult to precisely determine; however, they are not negligible for achieving highly precise Mo isotope analysis. In some previous studies for Os (OsO_3^-)[30] and Nd (NdO^+)[31] isotope analysis, the correction of O isotopic interferences was conducted by assuming a uniform O isotopic composition of Nier[32]: $^{17}O/^{16}O = 0.000375$ and $^{18}O/^{16}O = 0.002044$. Conversely, Luguet et al.[33] determined the in-run O isotope composition for each Os isotope measurement with N-TIMS by sampling $^{192}Os^{16}O_2{}^{17}O^-$ and $^{192}Os^{16}O_2{}^{18}O^-$ ions. The authors concluded that (1) the $^{18}O/^{16}O$ ratio can vary across multiple Os isotope measurements, and (2) the Nier's $^{17}O/^{16}O$ and $^{18}O/^{16}O$ ratios obviously deviated from the mass-dependent fractionation trend they obtained.

In this study, we conducted both correction methods for Mo isotope analysis, which are hereafter referred to as the "Nier's O" correction and the "In-run O" correction. In addition, we examined the "Mean O" correction method in which a uniform O isotopic composition determined by averaging multiple "In-run O" compositions was applied for correcting O isobaric interferences. The O isotope composition of MoO_3^- ions during each isotope measurement was determined by monitoring masses 148 ($^{100}Mo^{16}O_3^-$), 149

($^{100}Mo^{16}O_2{}^{17}O^-$), and 150 ($^{100}Mo^{16}O_2{}^{18}O^-$), and conducting the iterative calculations as described below. First, apparent isotopic ratios of $^{17}O/^{16}O$ (R_1) and $^{18}O/^{16}O$ (R_2) were determined:

$$R_1 = V_{149}/V_{148} \quad (1)$$

$$R_2 = V_{149}/V_{148} \quad (2)$$

where V_i represents the total ion beam intensity for the molecular mass of *i*. Next, the intensities of $^{j}Mo^{16}O_3^-$ ions (= I_j) were determined as follows.

$$I_{92} = V_{140} \quad (3)$$

$$I_{94} = V_{142} - I_{92} \times (3R_1^2 + 3R_2) \quad (4)$$

$$I_{95} = V_{143} - I_{92} \times (R_1^3 + 6R_1R_2) - I_{94} \times 3R_1 \quad (5)$$

$$I_{96} = V_{144} - I_{92} \times (3R_1^2R_2 + 3R_2^2) - I_{94} \times (3R_1^2 + 3R_2) - I_{95} \times 3R_1 \quad (6)$$

$$I_{97} = V_{145} - I_{92} \times 3R_1R_2^2 - I_{94} \times (R_1^3 + 6R_1R_2) - I_{95} \times (3R_1^2 + 3R_2) - I_{96} \times 3R_1 \quad (7)$$

$$I_{98} = V_{146} - I_{92} \times R_2^3 - I_{94} \times (3R_1^2R_2 + 3R_2^2) - I_{95} \times (R_1^3 + 6R_1R_2) - I_{96} \times (3R_1^2 + 3R_2) - I_{97} \times 3R_1 \quad (8)$$

$$I_{100} = V_{148} - I_{94} \times R_2^3 - I_{95} \times 3\,R_1R_2^2 - I_{96} \times (3R_1^2R_2 + 3R_2^2) - I_{97} \times (R_1^3 + 6R_1R_2) - I_{98} \times (3R_1^2 + 3R_2) \quad (9).$$

Similarly, the ion beam intensities of $^{100}Mo^{16}O_2{}^{17}O^-$ (= $I_{100}{}^{17}$) and $^{100}Mo^{16}O_2{}^{18}O^-$ (=$I_{100}{}^{18}$) were determined as follows:

$$I_{100}{}^{17} = V_{149} - I_{95} \times R_2{}^3 - I_{96} \times 3\,R_1R_2{}^2 - I_{97} \times (3R_1{}^2R_2 + 3R_2{}^2) - I_{98} \times (R_1{}^3 + 6R_1R_2) - I_{100} \times 3R_1 \quad (10)$$

$$I_{100}{}^{18} = V_{150} - I_{96} \times R_2{}^3 - I_{97} \times 3\,R_1R_2{}^2 - I_{98} \times (3R_1{}^2R_2 + 3R_2{}^2) - I_{100} \times (3R_1{}^2 + 3R_2) - I_{100}{}^{17} \times 3R_1 \quad (11).$$

Here, new oxygen isotope ratios were given by the following equations:

$$R_1' = I_{100}{}^{17}/I_{100} \quad (12)$$

$$R_2' = I_{100}{}^{18}/I_{100} \quad (13).$$

The new values R_1' and R_2' were compared with R_1 and R_2.

$$\Delta_{17} = R_1' - R_1 \quad (14)$$

$$\Delta_{18} = R_2' - R_2 \quad (15).$$

If either Δ_{17} or Δ_{18} was larger than 1×10^{-6}, then the calculations from equation (3) to (15) were repeated by replacing R_1 and R_2 with R_1' and R_2', respectively. In general, this

procedure was repeated three times to achieve $<1 \times 10^{-6}$. After the iterative calculations, the final R_1' and R_2' values were regarded as true O isotopic ratios, and the Mo isotope ratios were determined from I_{92}/I_{96}, I_{94}/I_{96}, I_{95}/I_{96}, I_{97}/I_{96}, I_{98}/I_{96}, and I_{100}/I_{96}. After the correction of O isotopic compositions, all Mo data were normalized to ^{96}Mo and corrected for mass-dependent fractionation via the exponential law of MoO_3 ions by assuming $^{98}Mo^{16}O_3/^{96}Mo^{16}O_3 = 1.453173$[34].

In the correction scheme for oxide interferences mentioned above, we assume that the isotopic composition of oxygen, which forms the molecular ion MoO_3^-, detected by Faraday cups is identical among different Mo isotopic species (e.g., $^{92}Mo^{16}O_2{}^{18}O/^{92}Mo^{16}O_3 = {}^{100}Mo^{16}O_2{}^{18}O/^{100}Mo^{16}O_3$). This is strictly incorrect because fractionation of Mo oxide ions occurs depending on their molecular masses until they are detected by Faraday cups. In the case of exponential law, we derive the following equation:

$$(^{92}Mo^{16}O_2{}^{18}O/^{92}Mo^{16}O_3) \times (m_{142}/m_{140})^{\alpha} = (^{100}Mo^{16}O_2{}^{18}O/^{100}Mo^{16}O_3) \times (m_{150}/m_{148})^{\alpha}, \quad (16)$$

where m stands for the molecular masses of MoO_3 and α is the fractionation factor. However, in our N-TIMS measurements of MoO_3^- ions, the magnitude of mass fractionation was in the range of $-0.3 < \alpha < 0.3$. With this range of mass fractionation factors, $(m_{150}/m_{148})^{\alpha}$ / $(m_{142}/m_{140})^{\alpha}$ varies from 0.9998 to 1.0002, which does not significantly affect the result of Mo isotope ratios when their analytical precisions are

considered.

After the correction scheme described above, Mo isotope ratios were obtained by averaging 360 ratios with 2σ rejection (rejecting 5% of the data). The precision of Mo isotopic ratios in a single isotope run is evaluated by 2 standard error (2SE) of the ratios within the 95% confidence interval. The Mo isotope ratios in samples are reported in the μ notation as follows:

$$\mu^{i}\mathrm{Mo} = \left\{ \frac{\left({}^{i}\mathrm{Mo}/{}^{96}\mathrm{Mo} \right)_{sample}}{\left({}^{i}\mathrm{Mo}/{}^{96}\mathrm{Mo} \right)_{std}} - 1 \right\} \times 10^{6} \qquad (17)$$

where *i* is the mass number and the subscript *std* represents the Kanto-Mo standard.

3. Results and Discussion

3.1. Optimization of MoO_3^- ionization

In N-TIMS, negative ions are produced on the surface of a hot metal filament. The ion yield β is theoretically described by the Langmuir–Saha equation for N-TIMS mode[35]:

$$\beta^- = \frac{1}{1+\frac{g_0}{g_-}exp\left(\frac{W-E_A}{kT}\right)} \quad (18)$$

where g_0/g_- is the ratio of the statistical weights of the neutral species and the ion, E_A is the electron affinity of the atom or molecule to be analyzed, W is the electron work function of the filament material used, T is the temperature in Kelvin, and k is the Boltzmann constant. According to the equation, the ionization efficiency (ion yield) can be improved by reducing the work function by choosing an optimal filament material and activator.

At first, we chose an activator that strengthened the MoO_3^- ion beam of four types of activators: $Ca(NO_3)_2$, $La(NO_3)_3$, $La(NO_3)_3$ + $Gd(NO_3)_3$, and $La(NO_3)_3$ + $Gd(NO_3)_3$ + $Ca(NO_3)_2$. The efficiencies were determined by integrating the total MoO_3^- ion beam intensities (500 ng of Mo) acquired with the initial filament temperature at 1210–1280 °C until all of the Mo on the filament has been exhausted. $La(NO_3)_3$ generated MoO_3^- ions more efficiently (at least 3.5 times) than the other activators. Although the $Gd(NO_3)_3$ activator was not particularly efficient to ionized MoO_3^- ions, it is most useful for

generating WO_3^-ions in the N-TIMS analysis[18].

To achieve the highest precision and analytical accuracy, selecting an appropriate activator/sample ratio that can sufficiently maintain the beam intensity is important. The detection efficiency of MoO_3^- drastically varied with the change in the La/Mo ratio on the filament (Figure 1). Irrespective of the amount of Mo used, the detection efficiency increased linearly at La/Mo <5 and stabilized at 5< La/Mo <7.5, although it decreased rapidly at La/Mo >7.5. Based on these results, we decided to use the $La(NO_3)_3$ solution as the activator, which achieved a ratio of La/Mo = 5 in the following experiments.

During the N-TIMS analysis, bleeding of O_2 gas increases the beam intensity for Os[30,36], Ru,[37] and W[18]. However, in the case of Mo, the more the partial pressure of O_2 in the sample chamber was increased (e.g., > 5×10^{-7} mbar), the more the MoO_3^-ion beam intensities deteriorated. Therefore, we did not apply O_2 gas bleeding for the analysis of Mo isotopes with N-TIMS.

3.2. Variation of oxygen isotopic compositions

The O isotopic interferences on MoO_3^- were traditionally corrected using a constant O isotopic composition such as the Nier's composition[23] or the IUPAC "best" composition[28]. However, these studies did not report the O isotopic composition actually observed during the individual Mo isotope measurement. As shown in Figure 2 and Table 2, our "In-run" O isotope composition (circles) varied slightly across different sample

measurements: $(3.874 \pm 0.002) - (3.885 \pm 0.002) \times 10^{-4}$ for $^{17}O/^{16}O$ and $(2.0583 \pm 0.0003) - (2.0685 \pm 0.0003) \times 10^{-3}$ for $^{18}O/^{16}O$ (errors are 2SE of the individual measurement). The average of 21 "In-run" O isotopic compositions obtained during the period of this study resulted in the "Mean" O isotopic composition (double circles) of which $^{17}O/^{16}O = (3.880 \pm 0.006) \times 10^{-4}$ and $^{18}O/^{16}O = (2.064 \pm 0.005) \times 10^{-3}$ (errors are 2SD). A much larger variation of the O isotopic composition was observed in some Os isotope studies in which oxygen was bled in the sample chamber while maintaining a constant gas pressure[33,38]. Oxygen isotopic variations were also observed in the study of W isotope analysis in which W isotopic compositions were controlled by the mass-dependent fractionation of oxygen isotopes[18].

The "In-run" O isotope ratios determined for the oxide interference correction in the calculation scheme of equations (1) to (15) represent the isotope ratios of oxygen that form MoO_3^- ions. They do not necessarily match the isotope ratios of the source oxygen for MoO_3 including O_2 gas remaining in the vacuumed sample chamber, the activator, and/or the sample solvent. This is because the equilibrium fractionation of O isotopes can occur between the source O_2 and MoO_3, the fractionation of which is controlled by isotope masses of atomic O (m = 16, 17, and 18). This type of fractionation is illustrated in Figure 2 as a dashed line passing through the "Mean" O data point. Similarly, fractionation of O isotopes would occur via kinetic processes of the source oxygen (e.g., evaporation) before the formation of MoO_3, in which case the trend of fractionation is indistinguishable from

that of equilibrium fractionation in Figure 2. In contrast, once MoO_3 has formed in the TIMS ion source, they fractionate as molecular ions of MoO_3^- until they are detected by Faraday cups, which is controlled by molecular masses of MoO_3 (m = 140–150). This type of fractionation is illustrated in Figure 2 as a thin line passing through the "Mean O" data point, which has a slope marginally different but nearly equal to the dashed line. In summary, the variation of "In-run" O isotopic composition observed in this study is attributed to the combination of three potential mass fractionation processes described above, which have mass fractionation trends nearly indistinguishable from one another in Figure 2.

Our "Mean" O isotope composition is slightly different from those of previous studies, including the Nier's O. We advocate that the deviation between the "Mean" O and the Nier's O compositions is possibly caused by large analytical uncertainties or inaccurate quantification of O isotopic compositions by Nier's study. In fact, O isotopic compositions, which are published by IUPAC, are plotted on our mass-fractionation line passing through the "Mean" O within the uncertainty (the error of $^{17}O/^{16}O$ for the IUPAC "best" value is ~9 $\times$ 10^{-7}) (Figure 2). Therefore, we believe that mass-independent fractionation or isobaric interference did not produce the deviation.

3.3. Molybdenum isotopic compositions in standard material

The Mo isotopic composition of our in-house standard Kanto-Mo has been

repeatedly analyzed (n = 21) with N-TIMS over the course of this study (Jan–March 2015). Table 3 summarizes the results obtained by applying the "Nier's O," "Mean O," and "In-run O" corrections.

3.3.1. "Nier's O" and "Mean O" corrections

In regards to the "Nier's O" correction, the reproducibilities (2 SD) of Mo isotope ratios for Kanto-Mo were 48, 13, 15, 23, and 46 ppm for $^{92}Mo/^{96}Mo$, $^{94}Mo/^{96}Mo$, $^{95}Mo/^{96}Mo$, $^{97}Mo/^{96}Mo$, and $^{100}Mo/^{96}Mo$, respectively. The consistent reproducibilities were obtained for the "Mean-O" correction. In contrast, all of the Mo isotopic ratios obtained by the "Mean-O" correction resulted in significant shifts from those of the "Nier's O" correction. This indicates that the "Mean-O" corrections are simply a linear shift of the Mo isotope ratios from those of the "Nier's O" correction. The Mo isotopic shift between the two correction methods is evaluated by modifying equation (17), in which case $(^{i}Mo/^{96}Mo)_{sample}$ and $(^{i}Mo/^{96}Mo)_{std}$ are replaced by $(^{i}Mo/^{96}Mo)_{Mean\text{-}O}$ and $(^{i}Mo/^{96}Mo)_{Nier's\ O}$, respectively. As shown in Table 3, the μ^{i}Mo(Mean/Nier) were 98, −11, 54, −104, and −105 ppm for $^{i}Mo = {}^{92}Mo$, ^{94}Mo, ^{95}Mo, ^{97}Mo, and ^{100}Mo, respectively. The shifts were clearly caused by the difference in the O isotopic composition used in the correction. However, geochemical applications of Mo isotopes commonly utilize the δ, ε, or μ notation in which the Mo isotope ratio in the sample of interest is expressed by the relative deviation ($\times 10^3$, 10^4, or 10^6, respectively) from that of a standard material[14]. In such cases, the two

correction methods are essentially identical.

3.3.2. "In-run O" correction

As noted above, we observed variable O isotopic compositions of MoO_3^- ions across multiple isotopic measurements, which is consistent with the case of Os isotope analysis with N-TIMS[33,38]. The Mo isotope ratios in Kanto-Mo obtained by the "In-run O" correction resulted in the following reproducibilities (2 SD): 47, 15, 10, 13, and 32 ppm for $^{92}Mo/^{96}Mo$, $^{94}Mo/^{96}Mo$, $^{95}Mo/^{96}Mo$, $^{97}Mo/^{96}Mo$, and $^{100}Mo/^{96}Mo$, respectively (Table 3). These are 1.0–1.8 times smaller than those obtained by the "Nier's O" and "Mean O" corrections, except for $^{94}Mo/^{96}Mo$.

In Figure 3, the $^{97}Mo/^{96}Mo$ ratios of Kanto-Mo obtained by the "Mean O" and "In-run O" corrections are plotted against the "In-run" $^{18}O/^{16}O$ values. Clearly, the "Mean O" $^{97}Mo/^{96}Mo$ increases as the $^{18}O/^{16}O$ increases (Figure 3a), whereas the variation of "In-run O" $^{97}Mo/^{96}Mo$ is independent to the $^{18}O/^{16}O$ value (Figure 3b). This indicates that the Mo isotopic composition measured using MoO_3ions with N-TIMS is strongly controlled by the "In-run" O isotopic compositions. We conclude that the Mo isotope measurement with N-TIMS requires the correction of O isotopic interferences using the O isotope composition obtained in individual isotope runs.

In addition to the three correction methods mentioned above, we examined the "Line-by-line O" correction in which the correction of O isotope interferences was

performed in individual data acquisition cycles (16.777 s) within a single isotopic run consisting of 360 cycles. The reproducibilities (2SD) of Mo isotope ratios in Kanto-Mo by this approach were 47, 16, 10, 13, and 33 ppm for $^{92}Mo/^{96}Mo$, $^{94}Mo/^{96}Mo$, $^{95}Mo/^{96}Mo$, $^{97}Mo/^{96}Mo$, and $^{100}Mo/^{96}Mo$, respectively. These are generally consistent with those obtained by the "In-run O" correction, but the "Line-by-line O" correction in theory provides a more accurate Mo isotopic composition. Therefore, in the following, we use the Mo isotope ratios in various samples obtained by the "Line-by-line O" correction. Note that the analytical uncertainties for all the μMo values were improved by 1.3–2.7 times compared to those of the standard measurements in previous studies conducted by MC-ICP-MS.[14,15] These studies reported that the external reproducibilities (2SD) of the standard (Alfa Aesar Mo) are 72, 43, 26, 21, and 43 ppm for $^{92}Mo/^{96}Mo$, $^{94}Mo/^{96}Mo$, $^{95}Mo/^{96}Mo$, $^{97}Mo/^{96}Mo$, and $^{100}Mo/^{96}Mo$, respectively (normalized to $^{98}Mo/^{96}Mo$).

3.3.3. Mass interferences and blanks

Potential isobaric interferences in the Mo isotope analysis with N-TIMS (e.g., Zr and Ru) would cause inaccurate results. Thus, special care is required to ionize Ru because (i) Ru can produce a strong RuO_3^- ion beam when using a Pt filament and $Ba(OH)_2$ activator[37], and (ii) the complete removal of Ru from Mo via ion exchange chromatography is difficult to achieve[15,27]. To evaluate the effect of isobaric interferences, the mixed solution (Mo standard solution containing 2% Zr or 2% Ru, which was assumed to be separated by the

two-stage chemical separation procedure[27]) was measured (Table 4). Within the uncertainty, the molybdenum isotopic ratios in the mixed solution were indistinguishable with those of the Kanto-Mo standard solution. The result indicates that the ionization of ZrO_3^- and RuO_3^- ions with the combination of Re filament and $La(NO3)_3$ activator is negligible compared to the ionization of MoO_3^- ions.

Molybdenum blanks during the N-TIMS analysis should cause unexpected isotopic shifts in Mo isotopic compositions, especially when analyzing isotopically anomalous extraterrestrial samples. The amount of Mo blank during the N-TIMS analysis was evaluated by loading 20 pg of the ^{97}Mo-enriched spike on the Re filament together with the $La(NO_3)_3$ activator. The filament temperature was increased as described in section 2.4.2 until the condition of sample measurement was met, and MoO_3^- ions were detected in the ion-counting mode using the central SEM. The amount of Mo blank during the N-TIMS analysis was calculated to be <56 pg by the isotope dilution method, assuming that the blank Mo has a terrestrial isotopic composition. The Mo blank has a negligible effect on the sample measurements examined in this study in which ~ 3000 ng of Mo was applied.

3.3.4. Accuracy of Mo isotope analysis

To evaluate the accuracy of our Mo isotope analysis, we measured the Mo isotope compositions of two synthesized solutions, Mix-A and Mix-B. The two solutions were artificially enriched in ^{92}Mo, ^{97}Mo, and ^{100}Mo compared to the Kanto-Mo solution. As

mentioned earlier, the absolute isotopic compositions of the two synthesized samples are difficult to determine precisely; however, the two samples were synthesized by gravimetrically mixing the Kanto-Mo solution and the mixed spike solution enriched in ^{92}Mo, ^{97}Mo, and ^{100}Mo in different proportions such that the μ^{92}Mo, μ^{97}Mo, and μ^{100}Mo values in Mix-A can be predicted from those obtained by the analysis of Mix-B and the weights of the starting materials. As shown in Table 4, the μMo values obtained by the analysis of Mix-A match those of the predicted values within the uncertainty, confirming the accuracy of our Mo isotope analysis.

To further evaluate the accuracy of our mass spectrometry technique, the Mo isotope composition in three terrestrial rocks (JB-3, JA-3, JR-2), two iron meteorites (Henbury and Albion), as well as new Mo isotopic data for IIIAB Tambo Quemado, was investigated (Table 4). Molybdenum isotopic compositions of terrestrial rocks were not distinct from those of Kanto-Mo within the uncertainties. In contrast, the iron meteorites are known to possess positive values in μ^{92}Mo, μ^{94}Mo, μ^{95}Mo, μ^{97}Mo, and μ^{100}Mo relative to the terrestrial standard[14,15]. As shown in Table 4 and Figure 4, we reproduced the positive μMo values associated with this meteorite. Molybdenum isotope anomalies for two iron meteorites, (Henbury and Albion) were consistent with previously reported values. In addition, new Mo isotopic compositions of IIIAB Tambo Quemado were determined here, which were identical to other IIIAB iron meteorites within uncertainty, including Henbury.

3.4. Application of the method

Extremely high precision isotope analysis for nontraditional transition metals (e.g., Mo, W) in terrestrial and extraterrestrial materials could provide new insights into the studies of dynamical and chemical processes in the early Solar System. For example, W isotopic analyses with less than 10 ppm of analytical precision revealed that the lunar mantle had a well-resolved ^{182}W excess of 20 ppm relative to the modern terrestrial mantle, which was caused by a giant impact and subsequent late veneer events[39,40]. Conversely, excluding some carbonaceous chondrites and iron meteorites, Mo isotope compositions in extraterrestrial materials are difficult to resolve from the terrestrial material at the current level of analytical precision with MC-ICP-MS[15]. Our mass spectrometric technique developed in this study has the potential to better discriminate the Mo isotope compositions in a variety of meteorites that would reflect the diversity of their origin in terms of time and space in the early Solar System.

4. Concluding Remarks

Based on this study, the following conclusions were reached:

(1) We examined four types of activators to evaluate the detection efficiencies of MoO_3^- ions with N-TIMS. The optimal condition to ionize Mo was to load Mo on a Re single filament together with $La(NO_3)_3$ so that La/Mo = 5.

(2) We discovered that the oxygen isotope composition of MoO_3^- ions significantly varied across different isotopic measurements. To achieve highly precise Mo isotope analysis, determining the in situ O isotope composition for each measurement and use the data to correct for the O isotope interferences is important, rather than utilizing a fixed O isotope composition throughout all measurements (e.g., Nier's O isotope composition[32]).

(3) The Mo isotopic ratios in the Kanto-Mo standard solution obtained by the in-situ O isotope correction resulted in the following reproducibilities: 47, 16, 10, 13, and 33 ppm for $^{92}Mo/^{96}Mo$, $^{94}Mo/^{96}Mo$, $^{95}Mo/^{96}Mo$, $^{97}Mo/^{96}Mo$ and $^{100}Mo/^{96}Mo$, respectively. The reproducibilities have been improved at least several times compared to those obtained in previous MC-ICP-MS studies.

(4) The accuracy of our technique was confirmed by measuring two synthesized solutions enriched with an abundance of ^{92}Mo, ^{97}Mo, and ^{100}Mo. In addition, the Mo isotope ratios in two iron meteorites Henbury (IIIAB) and Albion (IVA) obtained in this study

were consistent with those reported in a previous study[15]. In addition, Mo isotope ratios in a new iron meteorite, Tambo Quemado (IIIAB), were determined. Our N-TIMS technique is suitable for the studies of nucleosynthetic isotope anomalies in extraterrestrial materials as well as the mass-dependent Mo isotopic shift in environmental samples.

Acknowledgements

We are grateful to R.J. Walker for useful discussion. We thank T. Hirata and Y. Fukami for providing an iron meteorite sample. This research was supported by a grant for the Global COE Program, “From the Earth to Earths” from the Ministry of Education, Culture, Sports, Science, and Technology of Japan, and KAKENHI Grant Number 23340171 from the Japan Society for the Promotion of Science (JSPS).

References

(1) Böhkle, J.-K.; De Laeter, J. R.; De Bièvre, P.; Hidaka, H.; Peiser, H. S.; Rosman, K. J. R. Taylor, P. D. P. *J. Phys. Chem. Ref. Data*, **2005**, *34*, 57-67.

(2) Barling, J.; Arnold, G. L.; Anbar, A. D. *Earth Planet. Sci. Lett.*, **2001**, *193*, 447-457.

(3) Siebert, C.; Nägler, T. F.; von Blanckenburg, F.; Kramers, J. D. *Earth Planet. Sci. Lett.*, **2003**, *211*, 159-171.

(4) Siebert, C.; McManus, J.; Bice, A.; Poulson, R.; Berelson, W. *Earth Planet. Sci. Lett.*, **2006**, *241*, 723-733.

(5) Poulson, R. L.; Siebert, C.; McManus, J.; Berelson, W. M. *Geology*, **2006**, *34*, 617-620.

(6) Arnold, G. L.; Anbar, A. D.; Barling, J.; Lyons, T. W. *Science*, **2004**, *304*, 87-90.

(7) Nägler, T. F.; Siebert, C.; Lüschen, H.; Böttcher, M. E. *Chem. Geol.*, **2005**, *219*, 283-295.

(8) Neubert, N.; Nägler, T. F.; Böttcher, M. E. *Geology*, **2008**, *36*, 775-778.

(9) Duan, Y.; Anbar, A. D.; Arnold, G. L.; Lyons, T. W.; Gordon, G. W.; Kendall, B. *Geochim. Cosmochim. Acta*, **2010**, *74*, 6655-6668.

(10) Kendall, B.; Gordon, G. W.; Poulton, S. W.; Anbar, A. D. *Earth Planet. Sci. Lett.*, **2011**, *307*, 450-460.

(11) Zhang, Y.; Gladyshev, V. N. *J. Mol. Biol.*, **2008**, *379*, 881-899.

(12) Zerkle, A. L.; Scheiderich, K.; Maresca, J. A.; Liermann, L. J.; Brantley, S. L.

Geobiology, **2011**, *9*, 94-106.

(13) Bisterzo, S.; Gallino, R.; Straniero, O.; Cristallo, S.; Käppeler, F. *Mon. Not. R. Astron. Soc.*, **2011**, 418, 284-319.

(14) Dauphas, N.; Marty, B.; Reisberg, L. *ApJ*, **2002**, *565*, 640-644.

(15) Burkhardt, C.; Kleine, T.; Oberli, F.; Pack, A.; Bourdon, B.; Wieler, R. *Earth Planet. Sci. Lett.*, **2011**, *312*, 390-400.

(16) Trinquier, A.; Birck, J-. L.; Allègre, C. J. *ApJ*, **2007**, *655*, 1179-1185.

(17) Caro, G.; Bourdon, B.; Birck, J. -L.; Moorbath, S. *Geochim. Cosmochim. Acta*, **2006**, *70*, 164-191.

(18) Touboul, M.; Walker, R. J. *Int. J. Mass Spectrom.*, **2011**, *309*, 109−117.

(19) Murthy, V., R. *Geochim. Cosmochim. Acta*, **1963**, 27, 1171-1178.

(20) Yokoyama, T.; Fukami, Y.; Okui, W.; Ito, N.; Yamazaki, H. *Earth Planet. Sci. Lett.*, **2015**, *416*, 46-55.

(21) Völkening, J.; Köppe, M.; Heumann, K., G. *Int. J. Mass Spectrom. Ion Proc.*, **1991**, 107, 147-159.

(22) Völkening, J.; Köppe, M.; Heumann, K., G. *Int. J. Mass Spectrom. Ion Proc.*, **1991**, 107, 361-368.

(23) Becker, H.; Walker, R. J. *Nature*, **2003**, *425*, 152-155.

(24) Burkhardt, C.; Kleine, T.; Dauphas, N.; Wieler, R. *Earth Planet. Sci. Lett.*, **2012**, *357−358*, 298−307.

(25) Quitte, G.; Birck, J.,-L.; Capman, F.; Allègre, C., J. *Geostand. Newsl.*, **2002**, 26, 149-160.

(26) Fukami, Y.; Kimura, J.; Irisawa, K.; Yokoyama, T.; Hirata, T. *41st Lunar and Planetary Science Conference*, The Woodlands, Texas, March 1–5, 2010, #1649.

(27) Nagai, Y.; Yokoyama, T. *Anal. Chem.*, **2014**, *86*, 4856-4863.

(28) Wieser, M. E.; De Laeter, J. R.; Varner, M. D. *Int. J. Mass Spectrom.*, **2007**, *265*, 40-48.

(29) Nagai, Y.; Yokoyama, T. *44st Lunar and Planetary Science Conference*, The Woodlands, Texas, March 1−5, 2013, #2373.

(30) Yokoyama, T.; Rai, V. K.; Alexander, C. M. O.; Lewis, R. S.; Carlson, R. W; Shirey, S. B.; Thiemens, M. H.; Walker, R. J. *Earth Planet. Sci. Lett.*, **2007**, *259*, 567-580.

(31) DePaolo, D. J.; Wasserburg, G. J. *Geophys. Res. Lett.*, **1976**, *3*, 249-252.

(32) Nier A. O. *Phys. Rev.*, **1950**, *77*, 789-793.

(33) Lugdet, A.; Nowell, G. M.; Pearson, D. G. *Chem. Geol.*, **2008**, *248*, 342-362.

(34) Lu, Q.; Masuda, A. *Int. J. Mass Spectrom. Ion Process.*, **1994**, *130*, 65-72.

(35) Heumann, K. G.; Eisenhut, S.; Gallus, S.; Hebeda, E. H.; Nusko, R.; Vengosh, A.; Walczyk, T. *Analyst*, **1995**, 120, 1291-1299.

(36) Walczyk, T.; Hebeda E. H.; Heumann, K. G. *Fresenius J. Anal. Chem.*, **1991**, *341*, 537-541.

(37) Becker, H.; Walker, R. J. *Chem. Geol.*, **2003**, *196*, 43-56.

(38) Liu, Y.; Huang, M.; Masuda, A.; Inoue, M. *Int. J. Mass Spectrom. Ion Process.*, **1998**, *173*, 163-175.

(39) Touboul, M.; Puchtel, I. S.; Walker, R. J. *Nature*, **2015**, *520*, 530-533.

(40) Kruijer, T. S.; Kleine, T.; Fischer-Gödde, M.; Sprung, P. *Nature*, **2015**, *520*, 534-537.

(41) Wasserburg, G. J.; Jacobsen, S. B.; DePaolo, D. J.; McCulloch, M.T.; Wen, T. *Geochim. Cosmochim. Acta*, **1981**, *45*, 2311-2323.

(42) Reisberg, L.; Zindler, A. *Earth Planet. Sci. Lett.*, **1986**, *81*, 29-45.

(43) Thirlwall, M. F. *Chem. Geol.*, **1991**, *94*, 13-22.

(44) Griselin, M.; van Belle, J. C.; Pomies, C.; Vroon, P. Z.; van Soest, M. C.; Davies, G. R. *Chem. Geol.*, **2001**, *172*, 347-359.

(45) Harvey, J.; Baxter, E. F. *Chem. Geol.*, **2009**, *258*, 251-257.

Figure Captions

Figure 1. Detection efficiencies of MoO_3^- ions as a function of La/Mo ratio on the filament when loading 1000–4000 ng of the Mo standard with $La(NO_3)_3$.

Figure 2. Variation of O isotope ratios across multiple Mo isotope measurements with N-TIMS ("In-run" O, n = 21). The "Mean" O isotope ratios were obtained by averaging "In-run" O data. Diamond symbols represent the O isotope ratios from N-TIMS measurements in previous studies.[1,33,38,41-45] The Nier's O isotope ratios are from ref. 32. Dashed (gray) and thin (black) lines passing through the "Mean" O data point are mass fractionation trends of O isotopes for atomic oxygen (m = 16, 17, 18) and $^{100}MoO_3$ (m = 148, 149, 150), respectively.

Figure 3. Mo isotopic ratios ($^{97}Mo/^{96}Mo$) plotted against the in-situ O isotope ratios, i.e., $(^{18}O/^{16}O)_{In\text{-}run}$ used for the O interference corrections. (a) Mo isotopic ratios corrected by the "Mean" O, and (b) Mo isotopic ratios corrected by the "In-run" O. The light blue line represents the regression line calculated using ISOPLOT 3.00, including the errors of O isotopic ratios (2SE) and Mo isotopic ratios (2SE). .

Figure 4. $\mu^{95}Mo$ values for three iron meteorites (Henbury, Alibion, and Tambo Quemado) measured in this study. Those of the same iron meteorites (Henbury, Albion) obtained in a previous study (ref. 15) are also plotted. The upper gray band is the reproducibility (2SD) of $\mu^{95}Mo$ in the Kanto-Mo standard obtained by the

"Line-by-line" O correction at 10 ppm. The lower gray band represents the reproducibility of μ^{95}Mo in a standard obtained in ref. 15 at 26 ppm.

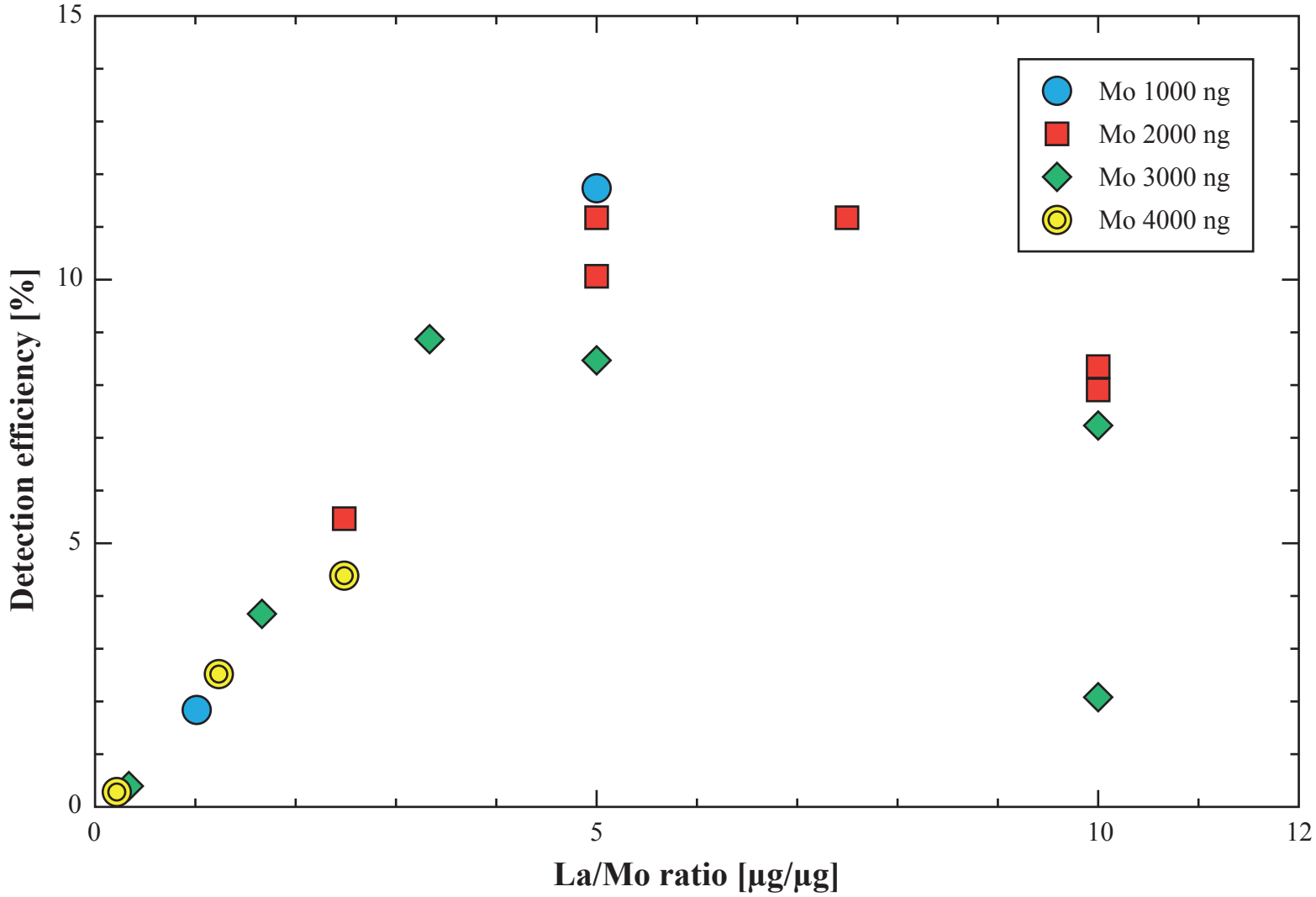

Figure 1

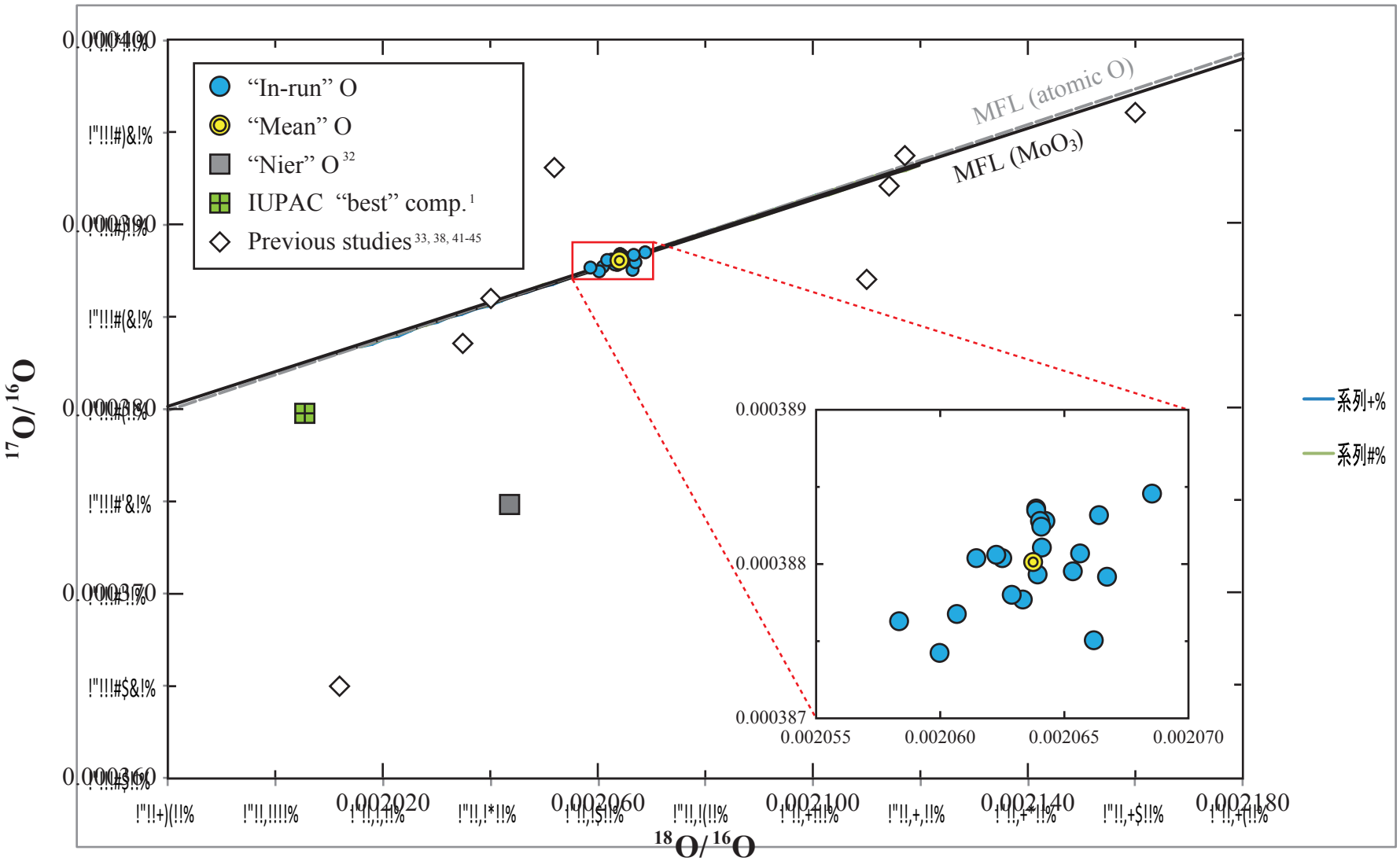

Figure 2

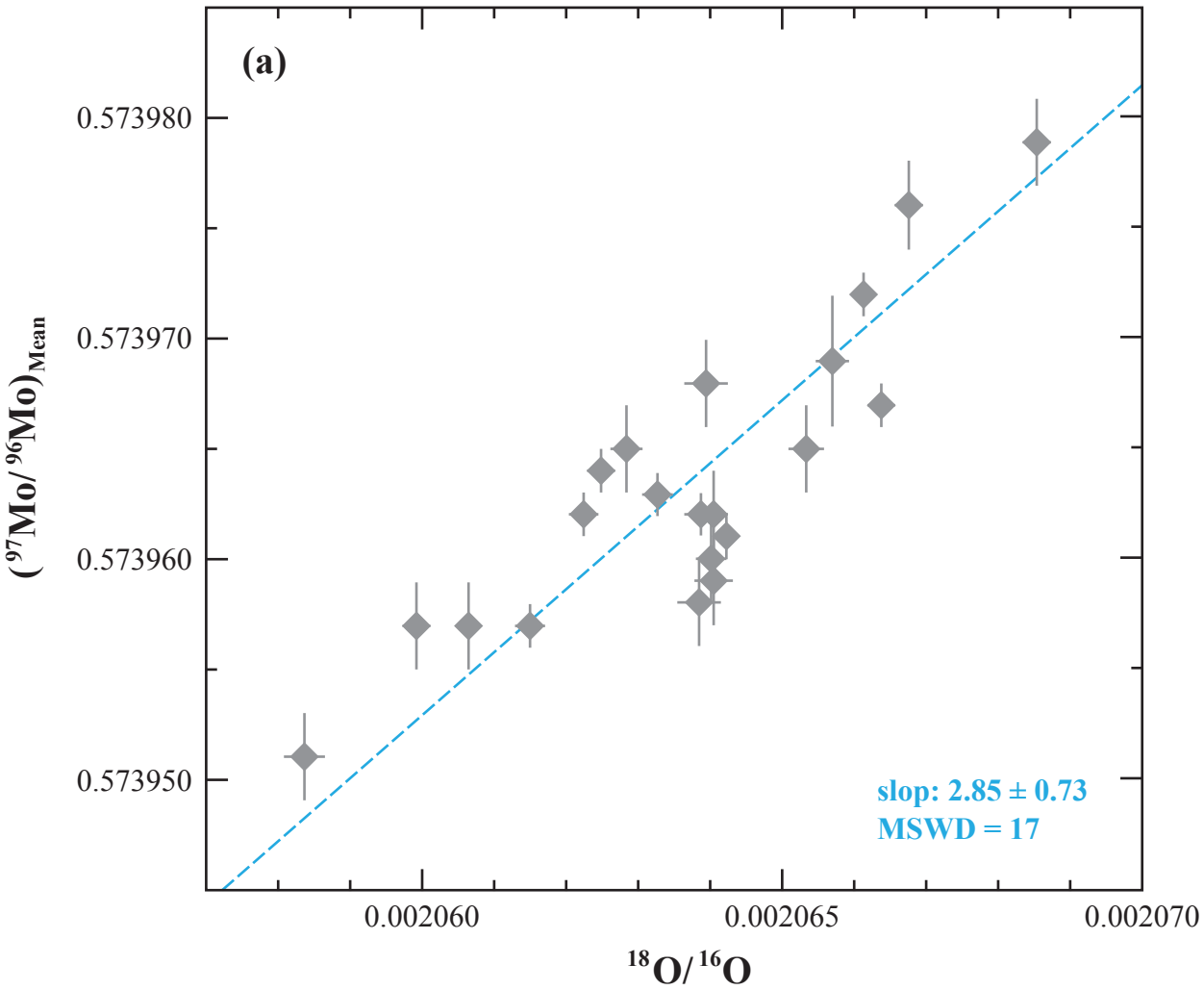

Figure 3a

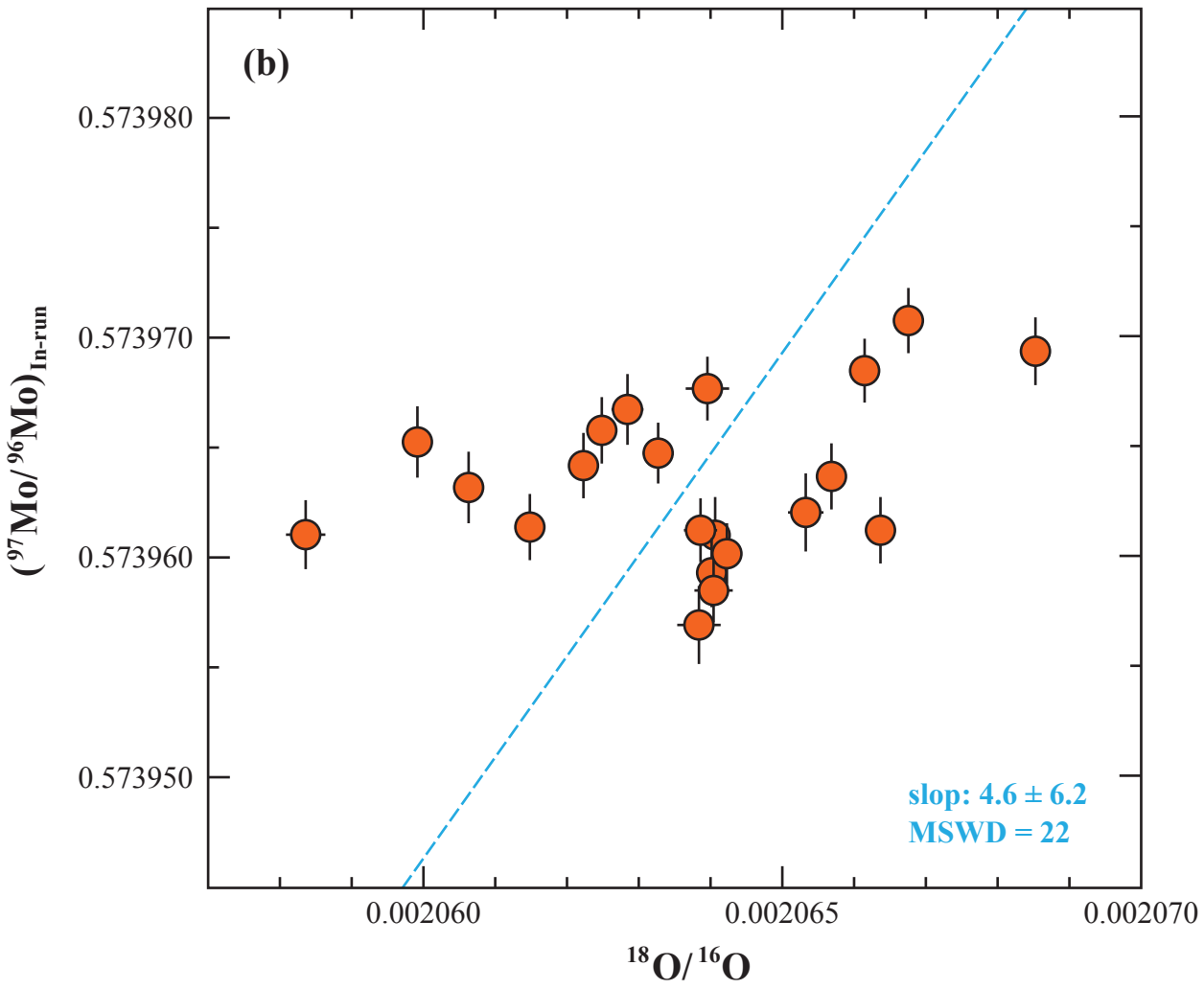

Figure 3b

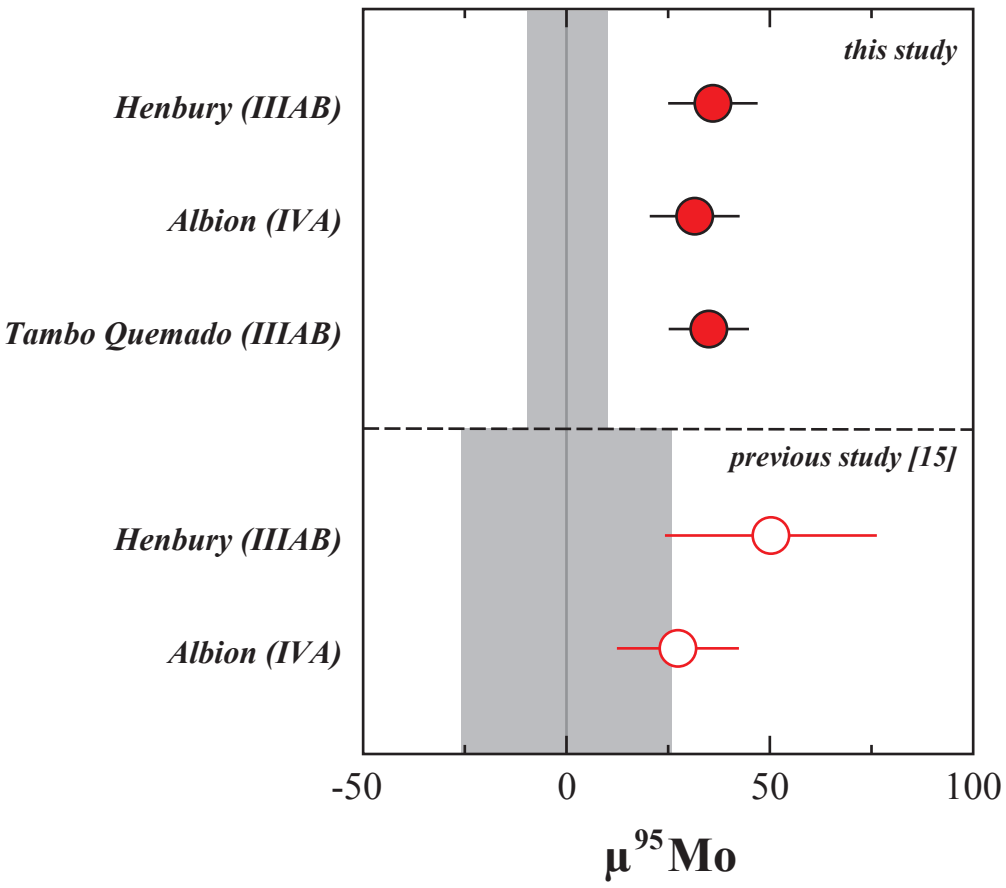

Figure 4

Table 1. Cup configuration of Mo isotopic analysis

cup	L4		L3	L2	L1	Center	H1		H2	H3	H4				
mass	140	141	142	143	144	145	146	147	148	149	150	151	152	153	154
	$^{92}Mo^{16}O_3^-$		$^{94}Mo^{16}O_3^-$	$^{95}Mo^{16}O_3^-$	$^{96}Mo^{16}O_3^-$	$^{97}Mo^{16}O_3^-$	$^{98}Mo^{16}O_3^-$		$^{100}Mo^{16}O_3^-$						
O isotope interferences															
		$^{92}Mo^{16}O_2{}^{17}O^-$		$^{94}Mo^{16}O_2{}^{17}O^-$	$^{95}Mo^{16}O_2{}^{17}O^-$	$^{96}Mo^{16}O_2{}^{17}O^-$	$^{97}Mo^{16}O_2{}^{17}O^-$	$^{98}Mo^{16}O_2{}^{17}O^-$		$^{100}Mo^{16}O_2{}^{17}O^-$					
			$^{92}Mo^{16}O_2{}^{18}O^-$		$^{94}Mo^{16}O_2{}^{18}O^-$	$^{95}Mo^{16}O_2{}^{18}O^-$	$^{96}Mo^{16}O_2{}^{18}O^-$	$^{97}Mo^{16}O_2{}^{18}O^-$	$^{98}Mo^{16}O_2{}^{18}O^-$		$^{100}Mo^{16}O_2{}^{18}O^-$				
			$^{92}Mo^{16}O^{17}O_2^-$		$^{94}Mo^{16}O^{17}O_2^-$	$^{95}Mo^{16}O^{17}O_2^-$	$^{96}Mo^{16}O^{17}O_2^-$	$^{97}Mo^{16}O^{17}O_2^-$	$^{98}Mo^{16}O^{17}O_2^-$		$^{100}Mo^{16}O^{17}O_2^-$				
				$^{92}Mo^{16}O^{17}O^{18}O^-$		$^{94}Mo^{16}O^{17}O^{18}O^-$	$^{95}Mo^{16}O^{17}O^{18}O^-$	$^{96}Mo^{16}O^{17}O^{18}O^-$	$^{97}Mo^{16}O^{17}O^{18}O^-$	$^{98}Mo^{16}O^{17}O^{18}O^-$		$^{100}Mo^{16}O^{17}O^{18}O^-$			
				$^{92}Mo^{17}O_3^-$		$^{94}Mo^{17}O_3^-$	$^{95}Mo^{17}O_3^-$	$^{96}Mo^{17}O_3^-$	$^{97}Mo^{17}O_3^-$	$^{98}Mo^{17}O_3^-$		$^{100}Mo^{17}O_3^-$			
					$^{92}Mo^{16}O^{18}O_2^-$		$^{94}Mo^{16}O^{18}O_2^-$	$^{95}Mo^{16}O^{18}O_2^-$	$^{96}Mo^{16}O^{18}O_2^-$	$^{97}Mo^{16}O^{18}O_2^-$	$^{98}Mo^{16}O^{18}O_2^-$		$^{100}Mo^{16}O^{18}O_2^-$		
					$^{92}Mo^{17}O_2{}^{18}O^-$		$^{94}Mo^{17}O_2{}^{18}O^-$	$^{95}Mo^{17}O_2{}^{18}O^-$	$^{96}Mo^{17}O_2{}^{18}O^-$	$^{97}Mo^{17}O_2{}^{18}O^-$	$^{98}Mo^{17}O_2{}^{18}O^-$		$^{100}Mo^{17}O_2{}^{18}O^-$		
						$^{92}Mo^{17}O^{18}O_2^-$		$^{94}Mo^{17}O^{18}O_2^-$	$^{95}Mo^{17}O^{18}O_2^-$	$^{96}Mo^{17}O^{18}O_2^-$	$^{97}Mo^{17}O^{18}O_2^-$	$^{98}Mo^{17}O^{18}O_2^-$		$^{100}Mo^{17}O^{18}O_2^-$	
							$^{92}Mo^{18}O_3^-$		$^{94}Mo^{18}O_3^-$	$^{95}Mo^{18}O_3^-$	$^{96}Mo^{18}O_3^-$	$^{97}Mo^{18}O_3^-$	$^{98}Mo^{18}O_3^-$		$^{100}Mo^{18}O_3^-$

Table 2. Oxygen isotopic ratios in the measurements

	$^{18}O/^{16}O$	2SE	$^{17}O/^{16}O$	2SE	reference
this study					
T0374F01	0.0020639	0.0000003	0.0003884	0.0000002	
T0374F02	0.0020641	0.0000002	0.0003882	0.0000002	
T0374F03	0.0020653	0.0000003	0.0003880	0.0000002	
T0374F04	0.0020640	0.0000003	0.0003881	0.0000002	
T0374F05	0.0020639	0.0000002	0.0003883	0.0000002	
T0374F06	0.0020664	0.0000002	0.0003883	0.0000002	
T0374F07	0.0020640	0.0000002	0.0003883	0.0000001	
T0385F01	0.0020583	0.0000003	0.0003876	0.0000002	
T0385F02	0.0020599	0.0000002	0.0003874	0.0000002	
T0385F03	0.0020657	0.0000002	0.0003881	0.0000002	
T0385F04	0.0020622	0.0000002	0.0003880	0.0000002	
T0385F05	0.0020640	0.0000003	0.0003879	0.0000002	
T0385F06	0.0020668	0.0000002	0.0003879	0.0000002	
T0385F07	0.0020629	0.0000002	0.0003878	0.0000002	
T0385F08	0.0020633	0.0000002	0.0003878	0.0000001	
T0385F09	0.0020661	0.0000002	0.0003875	0.0000002	
T0385F10	0.0020685	0.0000002	0.0003885	0.0000002	
T0390F01	0.0020615	0.0000002	0.0003880	0.0000002	
T0390F02	0.0020606	0.0000002	0.0003877	0.0000002	
T0390F03	0.0020625	0.0000002	0.0003880	0.0000002	
T0390F04	0.0020642	0.0000002	0.0003883	0.0000002	
average (2SD)	**0.0020637**	**0.0000048**	**0.0003880**	**0.0000006**	
previous studies					
	0.0020439		0.0003749		Nier (1950)[32]
	0.0021100		0.0003870		Wasserburg et al. (1981)[41]
	0.0021600		0.0003960		Nyquist in Wasserburg (1981)[41]
	0.0020120		0.0003650		Reisberg and Zindler (1986)[42]
	0.0021140		0.0003920		Thirlwall (1991)[43]
	0.0021171		0.0003936		Liu et al. (1998)[38]
	0.0020400		0.0003860		Griselin et al. (2001)[44]
	0.0020052		0.0003799		Böhlke et al. (2005)[1] *
	0.0020520		0.0003930		Harvey and Baxter (2009)[45]
	0.0020349		0.0003835		Luguet et al. (2008)[33]

* "Best measurement" value reported by IUPAC

Table 3. Molybdenum isotopic ratios corrected by four types of oxygen corrections

	$^{92}Mo/^{96}Mo$		$^{94}Mo/^{96}Mo$		$^{95}Mo/^{96}Mo$		$^{97}Mo/^{96}Mo$		$^{100}Mo/^{96}Mo$	
Nier O correction										
T0374F01	0.883137	0.000008	0.552482	0.000003	0.953195	0.000004	0.574017	0.000002	0.581539	0.000003
T0374F02	0.883141	0.000006	0.552484	0.000003	0.953201	0.000004	0.574022	0.000002	0.581536	0.000003
T0374F03	0.883138	0.000006	0.552484	0.000003	0.953198	0.000004	0.574025	0.000002	0.581544	0.000003
T0374F04	0.883153	0.000005	0.552484	0.000002	0.953204	0.000003	0.574019	0.000002	0.581537	0.000002
T0374F05	0.883143	0.000006	0.552483	0.000002	0.953199	0.000003	0.574022	0.000001	0.581534	0.000002
T0374F06	0.883160	0.000006	0.552493	0.000002	0.953199	0.000003	0.574026	0.000001	0.581549	0.000002
T0374F07	0.883149	0.000006	0.552488	0.000002	0.953201	0.000003	0.574020	0.000002	0.581541	0.000002
T0385F01	0.883187	0.000006	0.552483	0.000003	0.953221	0.000004	0.574011	0.000002	0.581532	0.000003
T0385F02	0.883131	0.000006	0.552477	0.000003	0.953217	0.000003	0.574017	0.000002	0.581530	0.000002
T0385F03	0.883156	0.000006	0.552491	0.000003	0.953210	0.000003	0.574029	0.000003	0.581555	0.000003
T0385F04	0.883173	0.000006	0.552487	0.000002	0.953215	0.000003	0.574021	0.000001	0.581544	0.000002
T0385F05	0.883136	0.000006	0.552485	0.000003	0.953206	0.000003	0.574027	0.000002	0.581559	0.000002
T0385F06	0.883114	0.000006	0.552488	0.000003	0.953204	0.000004	0.574036	0.000002	0.581564	0.000003
T0385F07	0.883140	0.000006	0.552483	0.000003	0.953212	0.000003	0.574024	0.000002	0.581546	0.000003
T0385F08	0.883137	0.000006	0.552485	0.000002	0.953202	0.000003	0.574023	0.000001	0.581550	0.000002
T0385F09	0.883102	0.000005	0.552480	0.000002	0.953196	0.000003	0.574031	0.000001	0.581551	0.000002
T0385F10	0.883099	0.000006	0.552487	0.000003	0.953196	0.000003	0.574038	0.000002	0.581565	0.000002
T0390F01	0.883136	0.000007	0.552485	0.000003	0.953207	0.000003	0.574017	0.000001	0.581520	0.000003
T0390F02	0.883138	0.000006	0.552482	0.000003	0.953211	0.000003	0.574017	0.000002	0.581517	0.000003
T0390F03	0.883122	0.000006	0.552482	0.000003	0.953208	0.000003	0.574023	0.000001	0.581525	0.000003
T0390F04	0.883115	0.000005	0.552482	0.000002	0.953200	0.000003	0.574021	0.000001	0.581535	0.000002
average*	**0.883138**	**0.000043**	**0.552485**	**0.000007**	**0.953205**	**0.000015**	**0.574023**	**0.000013**	**0.581542**	**0.000027**
reproducibility [ppm]	–	**48**	–	**13**	–	**15**	–	**23**	–	**46**
the Mean O correction										
T0374F01	0.883224	0.000008	0.552476	0.000003	0.953247	0.000004	0.573958	0.000002	0.581478	0.000003
T0374F02	0.883228	0.000006	0.552478	0.000003	0.953253	0.000004	0.573962	0.000002	0.581475	0.000003
T0374F03	0.883225	0.000006	0.552478	0.000003	0.953250	0.000004	0.573965	0.000002	0.581483	0.000003
T0374F04	0.883239	0.000005	0.552478	0.000002	0.953256	0.000003	0.573959	0.000002	0.581476	0.000002
T0374F05	0.883230	0.000006	0.552477	0.000002	0.953251	0.000003	0.573962	0.000001	0.581473	0.000002
T0374F06	0.883248	0.000006	0.552487	0.000002	0.953250	0.000003	0.573967	0.000001	0.581488	0.000002
T0374F07	0.883236	0.000006	0.552482	0.000002	0.953253	0.000003	0.573960	0.000002	0.581479	0.000002
T0385F01	0.883274	0.000006	0.552477	0.000003	0.953272	0.000004	0.573951	0.000002	0.581471	0.000003
T0385F02	0.883218	0.000006	0.552471	0.000003	0.953269	0.000003	0.573957	0.000002	0.581469	0.000002
T0385F03	0.883243	0.000006	0.552485	0.000003	0.953262	0.000003	0.573969	0.000003	0.581493	0.000003
T0385F04	0.883260	0.000006	0.552481	0.000002	0.953267	0.000003	0.573962	0.000001	0.581483	0.000002
T0385F05	0.883223	0.000006	0.552479	0.000003	0.953257	0.000003	0.573968	0.000002	0.581498	0.000002
T0385F06	0.883201	0.000006	0.552482	0.000003	0.953256	0.000004	0.573976	0.000002	0.581503	0.000003
T0385F07	0.883227	0.000006	0.552477	0.000003	0.953263	0.000003	0.573965	0.000002	0.581484	0.000003
T0385F08	0.883224	0.000006	0.552479	0.000002	0.953254	0.000003	0.573963	0.000001	0.581489	0.000002
T0385F09	0.883188	0.000005	0.552474	0.000002	0.953247	0.000003	0.573972	0.000001	0.581490	0.000002
T0385F10	0.883185	0.000006	0.552481	0.000003	0.953247	0.000003	0.573979	0.000002	0.581504	0.000002
T0390F01	0.883223	0.000007	0.552479	0.000003	0.953259	0.000003	0.573957	0.000001	0.581459	0.000003
T0390F02	0.883225	0.000006	0.552476	0.000003	0.953263	0.000003	0.573957	0.000002	0.581455	0.000003
T0390F03	0.883209	0.000006	0.552476	0.000003	0.953259	0.000003	0.573964	0.000001	0.581463	0.000003
T0390F04	0.883202	0.000005	0.552476	0.000002	0.953252	0.000003	0.573961	0.000001	0.581473	0.000002
average*	**0.883225**	**0.000043**	**0.552479**	**0.000007**	**0.953257**	**0.000015**	**0.573964**	**0.000013**	**0.581480**	**0.000027**
reproducibility [ppm]	–	**48**	–	**13**	–	**15**	–	**23**	–	**46**
μ^iMo(Mean/Nier) [ppm]	**98**		**-11**		**54**		**-104**		**-105**	
the in-run O correction										
T0374F01	0.883226	0.000008	0.552477	0.000003	0.953248	0.000004	0.573957	0.000002	0.581490	0.000003
T0374F02	0.883229	0.000006	0.552478	0.000003	0.953254	0.000004	0.573961	0.000002	0.581486	0.000003
T0374F03	0.883226	0.000006	0.552475	0.000003	0.953252	0.000004	0.573962	0.000002	0.581491	0.000003
T0374F04	0.883240	0.000005	0.552478	0.000002	0.953257	0.000003	0.573958	0.000002	0.581487	0.000002
T0374F05	0.883232	0.000006	0.552478	0.000002	0.953252	0.000003	0.573962	0.000001	0.581485	0.000002
T0374F06	0.883251	0.000006	0.552483	0.000002	0.953255	0.000003	0.573961	0.000001	0.581493	0.000002
T0374F07	0.883238	0.000006	0.552482	0.000002	0.953254	0.000003	0.573959	0.000002	0.581491	0.000002
T0385F01	0.883268	0.000006	0.552486	0.000003	0.953264	0.000004	0.573961	0.000002	0.581499	0.000003
T0385F02	0.883212	0.000006	0.552477	0.000003	0.953262	0.000003	0.573965	0.000002	0.581492	0.000002
T0385F03	0.883245	0.000006	0.552481	0.000003	0.953265	0.000003	0.573966	0.000003	0.581500	0.000003
T0385F04	0.883259	0.000006	0.552484	0.000002	0.953265	0.000003	0.573964	0.000001	0.581500	0.000002
T0385F05	0.883223	0.000006	0.552479	0.000003	0.953258	0.000003	0.573967	0.000002	0.581509	0.000002
T0385F06	0.883202	0.000006	0.552476	0.000003	0.953260	0.000004	0.573971	0.000002	0.581506	0.000003
T0385F07	0.883225	0.000006	0.552478	0.000003	0.953262	0.000003	0.573967	0.000002	0.581499	0.000003
T0385F08	0.883223	0.000006	0.552479	0.000002	0.953253	0.000003	0.573965	0.000001	0.581502	0.000002
T0385F09	0.883187	0.000005	0.552468	0.000002	0.953250	0.000003	0.573969	0.000001	0.581495	0.000002
T0385F10	0.883191	0.000006	0.552473	0.000003	0.953255	0.000003	0.573970	0.000002	0.581502	0.000002
T0390F01	0.883221	0.000007	0.552484	0.000003	0.953256	0.000003	0.573961	0.000001	0.581478	0.000003
T0390F02	0.883221	0.000006	0.552481	0.000003	0.953258	0.000003	0.573963	0.000002	0.581477	0.000003
T0390F03	0.883208	0.000006	0.552479	0.000003	0.953258	0.000003	0.573966	0.000001	0.581479	0.000003
T0390F04	0.883204	0.000005	0.552476	0.000002	0.953253	0.000003	0.573960	0.000001	0.581484	0.000002
average*	**0.883225**	**0.000041**	**0.552479**	**0.000008**	**0.953257**	**0.000010**	**0.573964**	**0.000008**	**0.581493**	**0.000019**
reproducibility [ppm]	–	**47**	–	**15**	–	**10**	–	**13**	–	**32**
μ^iMo(In-Run/Nier) [ppm]	**98**		**-11**		**54**		**-104**		**-84**	
the line-by-line O correction										
T0374F01	0.883227	0.000007	0.552477	0.000003	0.953248	0.000004	0.573957	0.000002	0.581477	0.000003
T0374F02	0.883229	0.000007	0.552478	0.000003	0.953254	0.000004	0.573961	0.000002	0.581474	0.000003
T0374F03	0.883225	0.000006	0.552475	0.000003	0.953252	0.000004	0.573962	0.000002	0.581478	0.000003
T0374F04	0.883240	0.000006	0.552477	0.000002	0.953257	0.000003	0.573959	0.000001	0.581475	0.000002
T0374F05	0.883231	0.000006	0.552478	0.000002	0.953252	0.000003	0.573961	0.000001	0.581472	0.000002
T0374F06	0.883251	0.000006	0.552483	0.000003	0.953254	0.000003	0.573961	0.000001	0.581480	0.000002
T0374F07	0.883238	0.000006	0.552482	0.000002	0.953253	0.000003	0.573959	0.000002	0.581478	0.000003
T0385F01	0.883268	0.000006	0.552487	0.000003	0.953264	0.000004	0.573961	0.000002	0.581486	0.000003
T0385F02	0.883212	0.000006	0.552477	0.000003	0.953262	0.000003	0.573965	0.000002	0.581479	0.000003
T0385F03	0.883246	0.000006	0.552480	0.000002	0.953266	0.000003	0.573964	0.000002	0.581488	0.000003
T0385F04	0.883261	0.000006	0.552484	0.000002	0.953265	0.000003	0.573964	0.000001	0.581487	0.000003
T0385F05	0.883223	0.000006	0.552478	0.000002	0.953258	0.000003	0.573968	0.000001	0.581499	0.000002
T0385F06	0.883203	0.000006	0.552476	0.000003	0.953259	0.000004	0.573971	0.000002	0.581495	0.000003
T0385F07	0.883224	0.000006	0.552479	0.000003	0.953261	0.000003	0.573967	0.000002	0.581487	0.000003
T0385F08	0.883223	0.000006	0.552479	0.000002	0.953252	0.000003	0.573965	0.000001	0.581490	0.000002
T0385F09	0.883186	0.000005	0.552467	0.000002	0.953250	0.000003	0.573968	0.000001	0.581483	0.000002
T0385F10	0.883193	0.000006	0.552473	0.000003	0.953255	0.000003	0.573969	0.000002	0.581489	0.000003
T0390F01	0.883221	0.000007	0.552484	0.000003	0.953255	0.000003	0.573961	0.000002	0.581465	0.000003
T0390F02	0.883221	0.000006	0.552481	0.000003	0.953257	0.000003	0.573963	0.000002	0.581465	0.000003
T0390F03	0.883209	0.000006	0.552479	0.000003	0.953258	0.000003	0.573966	0.000002	0.581466	0.000003
T0390F04	0.883205	0.000005	0.552476	0.000002	0.953253	0.000003	0.573960	0.000001	0.581472	0.000002
average*	**0.883226**	**0.000042**	**0.552479**	**0.000009**	**0.953256**	**0.000010**	**0.573963**	**0.000007**	**0.581480**	**0.000019**
reproducibility [ppm]	–	**47**	–	**16**	–	**10**	–	**13**	–	**33**
μ^iMo(Line-by-Line/Nier) [ppm]	**99**		**-11**		**54**		**-104**		**-105**	

* Erros of each measurement were 2 standard errors (2SE), but those of averages were 2 standard deviations (2SD).

Table 4. Molybdenum isotopic ratios of various kinds of samples

	n	μ^{92}Mo [a]	error [b]	μ^{94}Mo [a]	error [b]	μ^{95}Mo [a]	error [b]	μ^{97}Mo [a]	error [b]	μ^{100}Mo [a]	error [b]
standard (the line-by-line O)											
Junuary-March, 2015	*21*	-	± 47	-	± 16	-	± 10	-	± 13	-	± 33
standard Mo with 2% interference											
Mo + Zr	*3*	45	± 47	19	± 16	6	± 10	-8	± 13	-2	± 33
Mo + Ru	*3*	31	± 47	14	± 16	2	± 10	-5	± 13	5	± 33
artificial-spiked samples											
Mix-A (small)	*4*	140	± 47	8	± 16	5	± 10	47	± 13	66	± 33
Mix-B (large)	*4*	258	± 65	10	± 24	3	± 11	81	± 15	125	± 33
predict Mix-A from Mix-B		**130**	**± 33**	**5**	**± 12**	**1**	**± 6**	**40**	**± 8**	**63**	**± 17**
terrestrial rocks											
JA-3 (andesite)	*1*	17	± 36	2	± 13	1	± 8.7	3	± 0.9	13	± 15
JB-3 (basalt)	*1*	17	± 31	6	± 14	1	± 9.9	0	± 6.7	15	± 4.8
JR-2 (rhyolite)	*1*	12	± 36	4	± 13	2	± 8.7	0	± 0.9	-1	± 15
JR-2 duplicate	*1*	-6	± 31	0	± 14	0	± 9.9	-9	± 6.7	-8	± 4.8
terrestrial average [c]	***4***	**10**	**± 22**	**3**	**± 5.1**	**1**	**± 1.5**	**-1**	**± 10**	**5**	**± 22**
iron meteorites											
Tambo Quemade (IIIAB iron)	*3*	99	± 47	93	± 21	35	± 10	26	± 13	30	± 33
Henbury (IIIAB iron)	*2*	128	± 36	103	± 16	36	± 11	23	± 13	47	± 46
Albion (IVA iron)	*2*	88	± 36	74	± 16	31	± 11	12	± 13	16	± 46

[a] μiMo = [(iMo/96Mo)sample/(iMo/96Mo)std − 1] × 10^6: normalized to ^{98}Mo/^{96}Mo = 1.413173 by using the exponential law. The Mo isotopic ratios of the standard are the ones measured at measurement day.

[b] For samples measured more than twice, errors are the standard deviation from repeated analysis of standard solution or samples, whichever is larger. For samples measured once, errors are estimated by the standard deviation (2SD) from repeated analysis of the standard solution obtained at measurement day, which is larger than those of the 2SE.

[c] Errors were the standard deviations of terrestrial rocks (n=4; 2SD).